
Article:
De Santis, A., Ingham, D.B., Ma, L. et al. (1 more author) (2016) CFD analysis of exhaust gas recirculation in a micro gas turbine combustor for CO2 capture. Fuel, 173. C. pp. 146-154. ISSN 0016-2361

https://doi.org/10.1016/j.fuel.2016.01.063

CFD analysis of exhaust gas recirculation in a micro gas turbine combustor for CO_2 capture

Andrea De Santis[a,*], Derek B. Ingham[a], Lin Ma[a], Mohamed Pourkashanian[a]

[a] *Energy Engineering Group, Department of Mechanical Engineering, The Arts Tower, Western Bank, Sheffield, UK S10 2TN*

Abstract

The aim of this paper is to numerically investigate the effects of CO_2 dilution on the operation of an industrial micro gas turbine combustor in order to assess the possible application of exhaust gas recirculation (EGR) for post-combustion CO_2 capture. A complete 3D model of the combustion chamber has been developed, taking into account the conjugate heat transfer (CHT) and radiation effects, and a detailed chemical mechanism has been employed in the framework of the Flamelet Generated Manifolds approach to model the combustion process. The importance of including the effects of conjugate heat transfer in the model has been demonstrated for both air-fired and EGR conditions. Also, combustion with EGR resulted in lower temperature levels with respect to the air-fired case and thus in reduced NO_x production. Further, the increased presence of carbon dioxide has been observed to have an impact on both the flame speed and the flame stabilization mechanism.

According to the numerical results, EGR can be a viable way to increase the CO_2 content in the flue gas of dry low-emissions (DLE) combustors, and therefore enhance the efficiency of post-combustion carbon separation. At the same time, due to the reduced temperature levels within the combustion chamber, it is possible to attain lower NO_x emissions without compromising the combustion efficiency under the considered EGR levels.

Keywords: CFD, Carbon Capture and Storage, Exhaust gas recirculation, Flamelet Generated Manifolds

Nomenclature

c progress varialbe (-)

$\dot{m}$ mass flow rate (kg/s)

R EGR ratio (-)

*Corresponding author. Tel.: +39 0114 215 7220; E-mail address: adesantis1@sheffield.ac.uk

T temperature (K)

X_i mole fraction of species i (-)

Z mixture fraction (-)

Greek letters

δ_L laminar flame thickness (m)

ϕ equivalence ratio (-)

1. Introduction

A number of measures aimed at reducing greenhouse gas emissions from the energy sector have been proposed to tackle global warming and, at the same time, do not compromise economic growth. These measures include boosting the use of low-carbon power generation (nuclear, renewables), enhancing the efficiency of fossil fuel usage, reducing the energy demand through energy efficiency and deploying Carbon Capture and Storage (CCS). Among these possible solutions, CCS is particularly attractive because it allows us to preserve the economic value of fossil fuel reserves and infrastructures and also it is applicable to reduce industry-related emissions (IEA/UNIDO, 2013)

Although gas-fired power plants are less carbon-intensive than other forms of fossil fuel power generation, e.g. coal, gas is not a zero-emission fuel and therefore the application of CCS to gas-fired power plants has to be taken into account. Among all the possible carbon capture technologies that are suitable for gas-fired power generation, post combustion combined with exhaust gas recirculation is regarded as the most feasible in the short-term (Jansohn et al., 2011). The application of EGR results in a higher concentration of carbon dioxide in the exhaust gas and in a lower exhaust mass flow, which improves significantly the efficiency of the post-combustion capture process (Li et al., 2011).

From the combustion process point of view gas turbine operation with EGR differs from conventional air-firing, and this is mainly due to the increased CO_2 presence in the combustion environment. The presence of carbon dioxide has a significant impact on the combustion process in terms of temperature levels, heat transfer, flame stability and pollutant emissions (Røkke and Hustad, 2005).

The impact of carbon dioxide on the combustion process is due to both thermal and chemical effects (Habib et al., 2013). The thermal effects are related to the higher heat capacity of CO_2, which implies a reduction in the adiabatic temperature with respect to conventional air combustion. The chemical effects are related to the chemical reactivity of carbon dioxide and result both in a direct participation in elementary reactions and in an involvement in termolecular reactions as a third body with a higher efficiency with respect to nitrogen. It has been observed (Sabia et al., 2015) that the impact of the presence of carbon dioxide on the combustion chemistry is mainly due to the reaction:

$$CO + OH \leftrightarrows CO_2 + H \tag{1}$$

Let us consider the single most important chain-branching step in hydrocarbon combustion, i.e.:

$$H + O_2 \leftrightarrows OH + O \tag{2}$$

This reaction is fundamental since it generates the OH and H radicals necessary for the oxidation of fuel molecules. It can be seen that carbon dioxide decreases the production of these radicals by consuming the hydrogen radical available for reaction 2 via the reverse of reaction 1.

Andersson and Johnsson (2007) performed an experimental investigation in a 100 kW test facility, using an oxidizer consisting of a mixture of oxygen and carbon dioxide for two different compositions (the first with 21% O_2 and the second with 29% O_2) and the results obtained have been compared with a reference air-combustion case. In the 21% oxygen case, significantly lower temperature levels with respect to the reference air-fired case were observed, and this is mainly due to the higher heat capacity of carbon dioxide. In general, the lower temperature can be related also to an increase in radiation losses caused by the higher emissivity of carbon dioxide; the importance of radiative heat losses depends on the radiative characteristics of the considered flame. In the 29% O_2 case, the overall combustion process resulted in similar species concentrations and temperature levels as those observed in the air-combustion case. An increase in the flame radiation intensity up to 30% has been registered in this case compared to the baseline air-fired condition, despite the fact that the two cases were characterized by similar values of the temperature.

Baltasar et al. (1997) investigated the effects of EGR on the flame characteristics and pollutant emissions in a gas-fired laboratory furnace. The recirculated flue gas has been cooled down and the condensate water has been removed before its injection into the burner.

Three different values of the excess air have been considered, varying the EGR ratio from zero to the blow-off limit. The EGR ratio, R, is defined as

$$R = \frac{\dot{m}_{rec}}{\dot{m}_{air} + \dot{m}_{fuel}} \tag{3}$$

where $\dot{m}_{rec}$ is the mass flow rate of the flue gas being recirculated.

As reported in several other studies, e.g. Røkke and Hustad (2005), ElKady et al. (2009), Tanaka et al. (2013), a noticeable decrease in nitrogen oxides emissions can be obtained by recirculating the flue gas into the burner for all the excess air levels considered, the reduction being more significant for larger values of R. This is mainly due to the lower combustion temperature observed with EGR, and the consequent reduction of the thermal NO_x production. Flame blow-off has been observed to occur at an EGR ratio of about 0.3 for this particular furnace, regardless of the excess air level.

The effects of EGR in a DLE research combustor slightly modified from the version actually used in industrial gas turbines have been investigated by

ElKady et al. (2009). The oxidizer stream, consisting of an air/CO_2 mixture, is preheated to a temperature of 700 K at an inlet pressure of 10 atm. The aim was to demonstrate the feasibility of EGR in an existing DLE combustor in order to increase the carbon dioxide content in the flue gas to reduce the cost of the post-combustion CO_2 capture process. It has been demonstrated that an EGR ratio up to 35% (corresponding to a carbon dioxide content in the oxidizer and in the flue gas of about 3% and 10%, respectively) can be employed with minor changes in the combustion design with a significant reduction in NO_x emissions with respect to air-fired operation and slightly higher, but still acceptable, values for carbon monoxide emissions.

The feasibility of EGR in another industrial gas turbine combustor has been assessed by Tanaka et al. [8] with the aim of reducing NO_x emissions for Mitsubishi Heavy Industry's ultrahigh-temperature gas turbine (1700 C-class). Because, due the thermal NO_x formation path, nitrogen oxides production increases dramatically as the combustion temperature increases, NO_x production is a major issue for ultrahigh-temperature gas turbines. Under these conditions, EGR can be employed to reduce NO_x production by lowering the temperature in the combustion region. To investigate the effects of EGR on the NO_x formation, two different levels of oxygen in the oxidizer stream were considered: a high (19.6%) inlet O_2 concentration (corresponding to a 10% EGR ratio) and a low (17.0%) O_2 inlet concentration (corresponding to a 26.6% EGR ratio). A substantial decreasing in NO_x formation has been observed in the latter case, the nitrogen oxide production with a 26.6% EGR ratio being equal to 23% of that with 10% EGR ratio. No substantial differences in CO emissions have been observed between the two cases, and the CO levels were measured to be below the target of 10 ppm in both configurations.

Given the fact that EGR has a substantial impact on the combustion process, it is of paramount importance to evaluate the effects when considering its application to existing industrial gas turbine combustors. Due to the complexity of industrial configurations, experimental measurements within the combustion chamber are often not feasible (e.g.: Boudier et al. (2008)). For this reason, the development of accurate numerical models of the combustion process is essential in order to assess the possibility of operating the existing industrial gas turbine combustors with EGR.

In this paper, a molar concentration of 4% of CO_2 in the oxidizer stream (corresponding to an EGR ratio of about 35%) of the micro gas turbine Turbec T-100 combustion chamber has been considered, with the aim to evaluate the operation of this device in combination with EGR. The effects of carbon dioxide on the combustion process in terms of flame stability, heat release and pollutant emissions have been investigated, and a comparison with the operation of the same device without EGR has been performed.

2. Combustor description and numerical grid

The Turbec T-100 is a micro gas turbine system for the combined generation of heat and power (Ali et al., 2014). The nominal electrical power output is 100

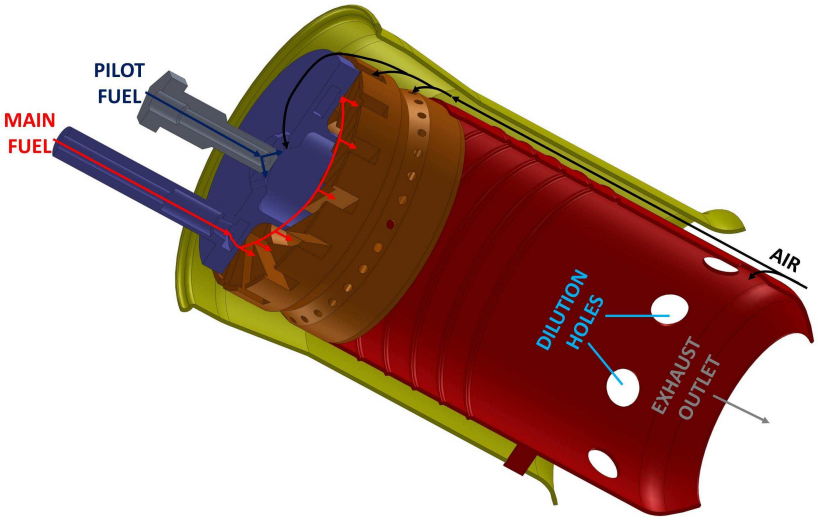

Figure 1: Section view of the CAD model for the Turbec T-100 combustor.

kW and the corresponding thermal power output is about 165 kW, with an electrical efficiency of about 33% and a 80% overall efficiency. This micro gas turbine employs a reverse flow DLE combustor. NO_x emissions are reduced by controlling the combustion temperature by means of a highly air-diluted lean premixed combustion process. Further, a non-premixed pilot flame is present to enhance flame stability. A section view of the CAD model of the combustor is shown in Figure 1.

With reference to the section view in Figure 1, the air coming from the compressor enters the combustion chamber through the annular section comprised between the outer casing (in yellow in Figure 1) and the flame tube (shown in red in the figure) and is split into a dilution stream, the mean combustion air and the pilot flame air.

The flame tube encompasses the main combustion process and is provided with nine dilution holes (9 x 19.6 mm) used to cool down the hot combustion products before the turbine inlet. The pilot fuel flows through a dedicated pipe and is injected into the pilot flame region using six nozzles (6 x 1 mm). The main fuel injection system (depicted in blue in Figure 1) is used for both supplying air to the pilot flame zone by means of 12 jet holes (12 x 3.5 mm) and to distribute the main fuel into a toroidal chamber. The main fuel is then injected from the toroidal chamber directly into the premixing vanes by means of 15 nozzles (15 x 1.2 mm).

The main swirler is equipped with 15 radial swirling vanes, where the premixing between the main fuel and the oxidizer takes place; further downstream, a series of 30 air jet holes distributed circumferentially is used to enhance turbulent mixing in the premixed mixture.

In order to minimize uncertainties coming from the boundary conditions be-

ing specified too close to the zone where chemical reactions are taking place, the entire combustor geometry has been included in the model, with some simplifying assumptions.

Mesh generation for industrial gas turbine combustors is particularly challenging due to the geometrical complexity of these devices. With the respect to the actual Turbec T-100 geometry, the following simplification have been made at the modelling stage: three pins used to connect the outer casing to the flame tube have been removed and the outer casing and the flame tube have been extended downstream to allow more room for dilution to take place. Also, the main fuel injection system has been simplified be removing the toroidal chamber; instead, a fully developed velocity profile boundary condition has been used for the fuel inlet, which consists of 15 nozzles issuing into an equal number of swirling vanes.

Further, all the solid parts have been included in the conjugate heat transfer calculations, with the exception of the outer casing walls which are regarded as being adiabatic.

In terms of meshing strategy, the complex regions encompassing the swirler and the fuel nozzles have been discretized employing an unstructured tetrahedral mesh. Prism layers have been generated on the walls of the unstructured region for a better prediction of the boundary layer physics. A structured hexahedral grid has been generated in the relatively simple region downstream of the swirler, including the air inlet section and the dilution holes. A conformal interface between the unstructured tetra-with-prisms region and the structured mesh has been generated using the advanced meshing capabilities of ANSYS ICEM CFD 15.0.

The mesh for the adiabatic cases consists of about 4.24M elements. Because conjugate heat transfer is expected to have a substantial impact on the heat transfer process, a second mesh consisting of about 6.25M elements (2.21M of them being solid cells) has been generated starting from the previous one and including the solid regions; this second grid has been used for the non-adiabatic cases. A mesh independence study has been performed using a grid of about 7.17M elements for the adiabatic case. All the most relevant monitored quantities have been found to differ by less than 2% between the different meshes.

3. Numerical models and simulation set up

All the numerical calculations have been performed using the CFD solver ANSYS Fluent 15.0.

The combustion system under consideration employs the lean premix technology to control the flame temperature and therefore reduce NO_x production. Because the operation point for this kind of combustors is close to the lean flammability limit, a non-premixed pilot flame is used to ensure combustion stability and prevent flame blow-out. For this reason, the combustion regime cannot be regarded as purely premixed, but falls into the definition of partially premixed combustion (Bilger et al., 2005); this regime, presenting features typ-

ical of both premixed and non-premixed flames, is the most challenging from the modelling point of view.

Further, the reactivity of CO_2 has an impact on the combustion chemistry at the level of radicals generation and consumption that has to be accounted for. Therefore, a detailed chemical mechanism has to be employed. In the present work all the simulations have been performed using the well-known GRI3.0 chemical mechanism (Gas Research Intitute, 2000), which describes the combustion of natural gas and comprises 325 reactions and 53 species, including the nitrogen chemistry.

The combustion process in the Turbec T-100 combustor falls into the *corrugated flamelet* and the *thin reaction zone* regimes on the Borghi diagram for turbulent premixed combustion regimes (Borghi, 1985). For this reason, a flamelet approach has been employed to model the combustion process. Within the flamelet approach, a turbulent flame is described as an ensemble of thin, laminar, one-dimensional flames, called flamelets, embedded within the turbulent flow. The standard flamelet approach employs a library of non-premixed flamelets generated using a counterflow configuration at different strain levels. On the other hand, premixed flamelets can be generated with a configuration consisting of one inlet in which the mixture is assumed to be perfectly mixed.

It has been shown (van Oijen, 2002) that using premixed flamelets is appropriate for modelling partially premixed combustion if the length associated with the mixture fraction gradient is larger than the flame thickness, i.e.

$$(\nabla Z \cdot \nabla Z)^{-0.5} \gg \delta_L \tag{4}$$

where ∇Z represents the mixture fraction gradient.

The condition represented by Equation 4 has been found to be satisfied in most of the computational domain (with the exception of a small region close to fuel and oxidizer inlets in the pilot region) for all the considered cases, due to the very strong turbulent mixing process which implies small mixture fraction gradient values. Under these conditions the combustion regime can be considered to be predominantly premixed and thus the use of premixed flamelets is more appropriate with respect to the standard approach of non-premixed flamelets.

The premixed flamelet library has been generated using the Flamelet Generated Manifold method (van Oijen and de Goey, 2000) solving species and energy transport equations for a freely propagating 1D premixed flamelets in the reaction progress space; details on the flamelet solver can be found in ANSYS, Inc. (2014). The turbulence-chemistry interaction has been taken into account using a presumed-PDF shape approach. The joint-PDF of reaction progress c and mixture fraction Z, used to evaluate the average scalar quantities by integration of the flamelet library, has been assumed to be equal to the product of two beta PDFs. In order to speed up the calculations, PDF integrations have been performed at the pre-processing stage and the results have been stored in a look-up table.

With respect to the turbulence modelling, it should be noted that the fluid dynamics in DLE combustors is characterized by complex phenomena such as

swirling flows, vortex breakdown and flow recirculation. The standard $k-\varepsilon$ model is known to perform poorly in the presence of flow separation and streamlines curvature (Jakirlic et al., 2002). The main cause for this is the linear relationship between the Reynolds stresses and the main flow field which implies isotropy of the turbulent viscosity, whilst such flows are characterized by a strong stress anisotropy. For this reason, the realizable $k-\varepsilon$ (Shih et al., 1995) has been employed in the present work. The realizable $k-\varepsilon$ is able, to same extent, to account for stress anisotropy. Also, the well-known round-jet anomaly of the standard model is overcome in the realizable version. This can be important in the modelling of DLE combustors, which normally feature a large number of fuel jets issuing into the premixing chamber.

The radiative transfer equation has been solved using the Discrete Ordinates approach. The mixture emissivity has been evaluated using the Weighted Sum of Grey Gas Model (WSGGM) with the default coefficients implemented in ANSYS Fluent (Smith et al., 1982).

With respect to nitrogen oxides prediction, it has to be noted that an accurate quantitative calculation of NOx production is an extremely challenging task. The methodology adopted in the present work is based on post-processing of the calculated flow-field and is aimed to predict NOx variation trends rather than provide precise quantitative figures, in order to assess the effects of EGR operation on pollutant emissions. Nevertheless, the calculated average NOx concentration at the combustor outlet for the baseline case agrees with the data provided by the manufacturer for the combustion chamber.

Thermal NO_x reaction rates have been evaluated using rate coefficients from Hanson and Salimian (1984). Prompt NO_x production has been calculated using a global kinetic model proposed by De Soete (1975) for C_2H_4-air flame, and a correction function to account for alkane hydrocarbon fuels different from ethylene has been employed, as described in ANSYS, Inc. (2014). Further, NO_x formation due to the N_2O-intermediate mechanism has been evaluated using the kinetic rate constants provided by Malte and Pratt (1975).

Also, NO_x reburn has been accounted for by assuming a general reburning mechanism having the form

$$CH_i + NO \rightarrow HCN + products \tag{5}$$

Reburn reactions from CH, CH_2 and CH_3 have been considered, with rate constants taken from Bowman (1991).

Both the air-fired and the EGR cases have been simulated at the nominal power output of 100 kW_e. The related absolute operating pressure is equal to 4.5 bar.

The boundary conditions employed for the air-fired case are summarised in Table 1. The fuel is assumed to be pure methane and the equivalence ratio (not including the dilution air in the calculation of the oxidizer mass flow rate) is equal to 0.44.

As mentioned above, combustion with EGR has been simulated by diluting the oxidizer stream with 4% carbon dioxide. The fuel and oxidizer mass flow

	$\dot{m}$ (kg/s)	X_i (-)	T (K)
Main fuel inlet	0.005431	X_{CH_4}: 1	288
Pilot fuel inlet	0.000948	X_{CH_4}: 1	288
Air inlet	0.6825	X_{O_2}: 0.207	863
		X_{N_2}: 0.793	

Table 1: Baseline air-fired boundary conditions.

	$\dot{m}$ (kg/s)	X_i (-)	T (K)
Main fuel inlet	0.005431	X_{CH_4}: 1	288
Pilot fuel inlet	0.000948	X_{CH_4}: 1	288
Air inlet	0.6825	X_{O_2}: 0.199 X_{N_2}: 0.761	863
		X_{CO_2}: 0.04	

Table 2: CO_2 injection case boundary conditions.

rates and temperature have been kept constant with respect to the baseline air-fired case. The resulting boundary conditions are reported in Table 2.

The emissivity has been considered to be constant and equal to 0.9 for all the walls (Dodds and Bahr, 1990).

The mixture density is retrieved directly from the look-up table generated by integration of the laminar flamelet library. Given the very lean overall equivalence ratio and the relatively low level of CO_2 dilution considered, thermal conductivity and molecular viscosity are considered to be equal to those of air. Values for molecular transport properties have been taken from Kadoya et al. (1985).

4. Results and discussion

4.1. Baseline case

The results obtained for the baseline air-fired case will be analysed in the present section. With respect to the heat transfer modelling, three different calculations have been carried out for both the baseline and the EGR cases: (i) adiabatic, (ii) non-adiabatic including conjugate heat transfer and (iii) non-adiabatic taking into account CHT and radiative heat transfer.

The flame in DLE combustors, such as the one employed in the Turbec T-100, is swirl stabilized. This means that the flame is stabilized by means of a recirculation zone generated by vortex breakdown of the swirling flow issuing from the premixing chamber.

Although many possible configurations are possible for swirl-stabilised flames (Chterev et al., 2014), the main expected features of the time-averaged flow field are common to all the configurations and consist of (see Figure 2): a toroidal outer recirculation zone (ORZ) generated by the rapid expansion of the swirling flow in the combustion chamber and confined by the walls of the chamber itself

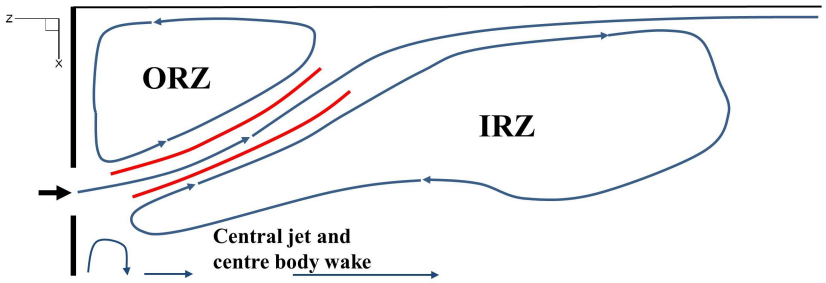

Figure 2: Main flow field features for a typical swirl stabilized flame.

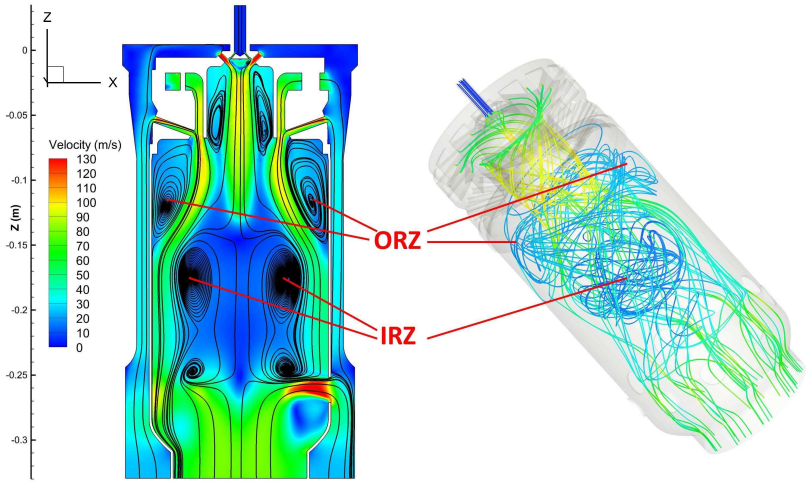

Figure 3: Air-fired case: velocity magnitude (with 2D streamlines) contours on the combustor mid-plane and 3D streamlines within the combustion chamber coloured by velocity magnitude.

and an inner recirculation zone (IRZ) due to the vortex breakdown mechanism. A high velocity jet issues between the ORZ and the IRZ. Two shear layers, highlighted in red in Figure 2, separate this jet from the recirculation zones. A central jet and a centre body wake might be present depending on the design of the central part of the combustor and on the possible presence of a pilot flame.

The mean velocity magnitude contours (including 2D streamlines) on the combustor mid-plane and 3D streamlines within the combustion chamber are shown in Figure 3 for the adiabatic baseline case. The typical flow field of DLE combustors can be observed, indicating that the realizable $k-\varepsilon$ is able to reproduce the main expected flow field features, at least from a qualitative point of view. Further, the presence of the pilot jet flame generates two small recirculation zones in the pilot region. Most of the combustion process takes place in the shear layers associated with the inner and outer recirculation zones and the pilot jet structure, where the mixing is particularly intense.

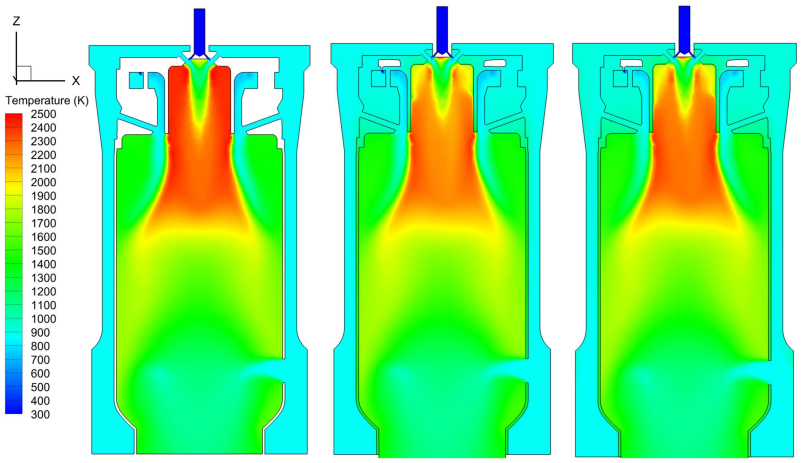

Figure 4: Air-fired case: temperature contours on the combustor mid-plane. From left to right: adiabatic, CHT, CHT with radiation.

Temperature contours on the combustor mid-plane for the adiabatic calculation, as well as for the CHT and the CHT including radiative heat transfer cases, are shown in Figure 4. As expected, taking into account the conjugate heat transfer has a significant impact on the temperature field, especially in the pilot region, as it will be discussed more in detail for the EGR case results. This is due to the very compact geometry of the device, which results in high temperature gradients and therefore in non-negligible conductive heat transfer through the walls. This effect is particularly evident in the pilot region, where thin walls separate the hot pilot flame zone from the relatively cold premixing chamber. Overall, the main conjugate heat transfer effect is to lower the temperature within the flame. The radiative heat transfer has a much smaller impact on the temperature field with respect to the CHT. This can be due to the small dimensions of the combustor and to the relatively low levels of CO_2 and H_2O reached within the flame. Faintly higher average temperature values, can be observed when radiative heat transfer is taken into account, as will be shown more in detail when analysing the numerical results with EGR.

The exhaust gas composition, turbine inlet temperature and maximum temperature within the combustor are reported in Table 3. The main species concentrations at the combustor outlet are not affected by including CHT and radiation in the calculations. On the other hand, the effect of CHT is to reduce the temperature at the walls and within the flame. This, in turn, has an impact on pollutant emissions. NO_x production is reduced as a consequence of the lowered temperature, due to the smaller contribution of the thermal mechanism in the nitrogen oxide formation.

Carbon monoxide levels are similar to those measured by ElKady et al. (2009) and Tanaka et al. (2013), and below the maximum level of 15 ppm reported by the manufacturer. The calculated NO_x content in the exhaust gas

	Adiabatic	CHT	CHT + radiation	
$\mathbf{O_2}$	17.08	17.08	17.08	17.09*
$\mathbf{CO_2}$	1.64	1.65	1.65	1.65*
$\mathbf{H_2O}$	3.31	3.31	3.31	3.32*
$\mathbf{NO_x}$ **(ppmv)**	16	7	9	$<$ 15**
CO(ppmv)	6	2	3	$<$ 15**
$\mathbf{T_{out,av}}$ **(K)**	1240	1237	1235	1233**
$\mathbf{T_{max}}$ **(K)**	2501	2462	2445	2540***

Table 3: Air-fired case: exhaust gas composition (mole fractions), average outlet temperature and peak temperature in the computational domain (*stoichimetric calculations - **manufacturer data - ***calculated adiabatic flame temperature).

is slightly higher when radiative heat transfer is accounted for, probably due to the faintly higher temperature in the flame region.

4.2. EGR case

EGR has been simulated by considering a 4% CO_2 dilution in the oxidizer stream and keeping the mass flow rates constant, as reported in Table 2. Further, the same three calculations as for the baseline case have been performed (i.e. adiabatic, CHT, CHT including radiation).

As broadly reported in the literature, e.g. Hinton and Stone (2014), carbon dioxide dilution has the effect of lowering the flame speed. Laminar flame speed values for the baseline and the EGR cases under the considered temperature and pressure levels have been calculated for 1D freely propagating premixed flames using Cantera (Goodwin et al., 2015) with the same chemical mechanism employed for the CFD calculations. A comparison of the laminar flame speed values calculated with Cantera for a CH_4-CO_2-O_2 mixture at 0.1MPa and 300 K with the experimental measurements from Xie et al. (2013) at two different CO_2 dilutions levels is shown on the left hand side of Figure 5. The comparison with the experimental data shows that the GRI3.0 mechanism is suitable to evaluate the laminar flame speed of methane flames in presence of CO_2 dilution at adiabatic flame temperature levels similar to those observed in the Turbec T-100 combustor for the baseline and the EGR cases (i.e. around 2450 and 2550 K).

The obtained laminar flame speed values obtained for the baseline and the EGR cases as a function of the equivalence ratio are shown on the right hand side of Figure 5. It is observed that the laminar flame speed peaks at a slightly rich condition, corresponding to an equivalence ratio ϕ = 1.05-1.1, in both cases. However, the maximum value for the EGR case is reduced by about 21% with respect to the air-fired cases, from 1.56 m/s to 1.23 m/s. Also, as an effect of the laminar flame speed reduction, the flammability range is reduced in the EGR case.

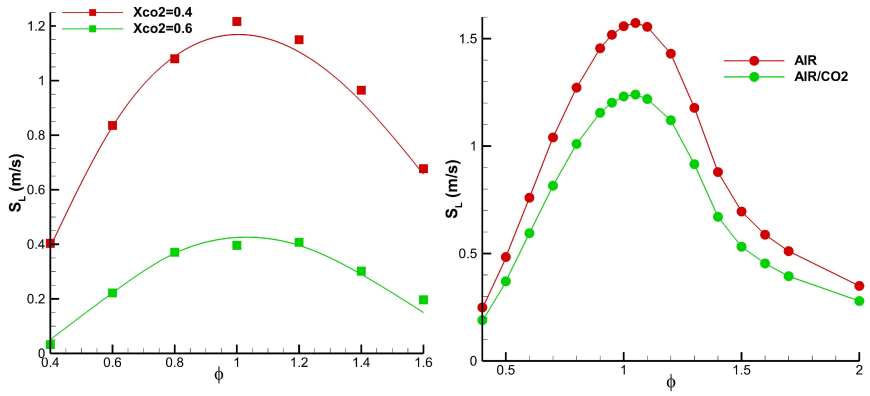

Figure 5: Calculated (lines) and measured from Xie et al. (2013) (squares) laminar flame speed values as a function of the equivalence ratio for a CH_4-CO_2-O_2 mixture (left-hand side) and calculated values (circles: calculated points) for the baseline and the EGR cases (right-hand side).

The effects of CO_2 dilution on the laminar flame speed have an impact on the flame speed profiles within the combustor. A plot of the flame speed along the combustor axis for both cases is reported on the left hand side of Figure 6; it can been observed that the EGR cases is characterized by lower flame speed values with respect to the air-fired case. Also, carbon dioxide dilution affects the velocity field, due to its the higher density with respect to nitrogen and to the different temperature field which affects the density of the mixture. The calculated axial velocity profiles along the combustor axis are shown on the right hand side of Figure 6; it can be seen that the location of the stagnation point, and thus the extent of the IRZ, is different between the air-fired and the EGR cases.

Also, as a combined effect of the different flame speed and velocity field, the axial location of the flame stabilization point (i.e. the point where the flame speed is equal to the axial velocity) is different in the two cases. The calculated distance of the axial flame stabilization point from the swirler outlet plane for all the considered cases is reported in Table 4. CO_2 dilution has been found to move the flame stabilization point around 0.8-0.9 cm closer to the swirler outlet section with respect to the baseline case in all the considered calculations (adiabatic, CHT, and CHT with radiative heat transfer). The impact of the conjugate heat transfer is much smaller (the flame stabilization point has been observed to be moved 2-3 mm closer to the swirler outlet with respect to the adiabatic calculations in both the baseline and the EGR cases), whilst the effect of radiative heat transfer on the flame stabilization location is negligible.

Temperature contours for the EGR case on the combustor mid-plane are shown in Figure 7. A comparison with the temperature contours reported in Figure 4 shows how the most evident effect of EGR is to lower the temperature levels in the flame region. A radial temperature plot at the axial location Z =

	Baseline	EGR
Adiabatic	0.068	0.060
CHT	0.072	0.063
CHT + RHT	0.072	0.064

Table 4: Calculated distance (m) of the axial flame stabilization point from the swirler outlet plane.

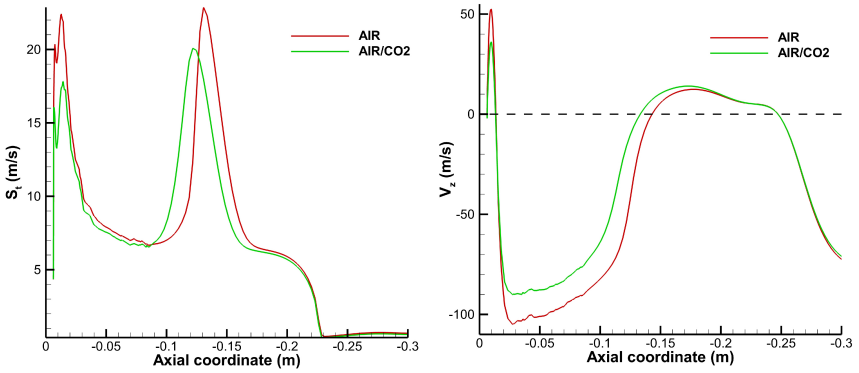

Figure 6: Axial profiles of the turbulent flame speed (left) and axial velocity component (right) for the baseline CHT and the EGR CHT cases.

-0.09 m, i.e. 2.5 cm downstream of the swirler outlet section, for the baseline and the EGR cases including CHT, as well as for the EGR case including both CHT and RHT, is shown on the left hand side of Figure 8. The temperature reduction due to CO_2 dilution in the hot flame region, and in the relatively colder central region associated with the pilot jet wake, can be observed.

Also, the faint temperature increase within the flame due to radiative heat transfer mentioned for the air-fired case can be seen in the EGR case as well. This latter effect is related to radiative heat flux coming from the hot walls being absorbed in the gas mixture.

Since EGR leads to a higher concentration of CO_2 and H_2O in the flame region, theoretically the radiative heat transfer should be enhanced in this case. However, a negligible increase in the radiative heat transfer has been observed under the considered conditions; this can be due to the relatively small CO_2 dilution considered, as well as to the small dimensions of the combustion chamber and to the fact that the absorption coefficients from Smith et al. (1982) have been calculated under air-fired conditions, and thus might not be accurate for EGR combustion (Clements et al., 2015).

Also, similarly to the air-fired case, it has been observed that the impact of CHT on the temperature field is significant, especially in the pilot flame region. A radial temperature plot within the pilot region at Z = -0.04 m (the location of this axial position is shown in Figure 7) for the adiabatic and CHT calculations

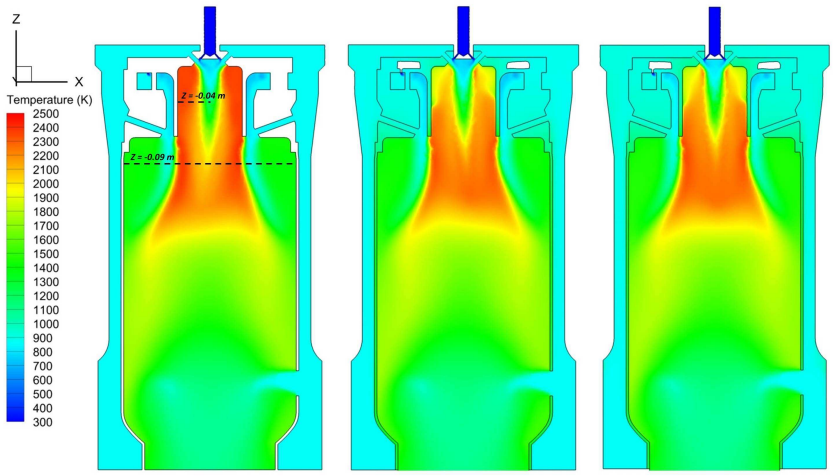

Figure 7: EGR case: temperature contours on the combustor mid-plane. From left to right: adiabatic, CHT, CHT with radiation.

for the EGR case is reported on the right hand side of Figure 8, to highlight the effects of conjugate heat transfer. The calculated wall temperature in the adiabatic case is very high (the wall location corresponds to X = 0.0255 m in the plot), and beyond the structural limit for steel. It can be observed that CHT has the effect of reducing the wall temperature significantly, to a value slightly above 1000 K.

The flue gas composition, along with the average outlet temperature and the peak temperature in the computational domain for the EGR case are reported in Table 5.

The same general observations made for the air-fired case also apply to the EGR case. From a comparison with the figures reported in Table 3 for the

	Adiabatic	**CHT**	**CHT + radiation**	
$\mathbf{O_2}$	16.19	16.19	16.19	16.19*
$\mathbf{CO_2}$	5.61	5.62	5.62	5.62*
$\mathbf{H_2O}$	3.36	3.37	3.37	3.37*
$\mathbf{NO_x}$ **(ppmv)**	11	4	5	n.a.
CO(ppmv)	9	5	5	n.a.
$\mathbf{T_{out,av}}$ **(K)**	1238	1235	1233	n.a.
$\mathbf{T_{max}}$ **(K)**	2429	2395	2405	2471**

Table 5: EGR case: exhaust gas composition (mole fractions), average outlet temperature and peak temperature in the computational domain (*stoichiometric calculations - **calculated adiabatic flame temperature).

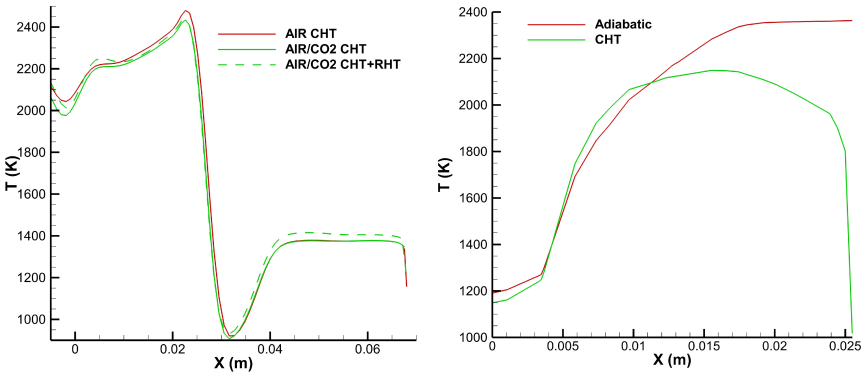

Figure 8: Radial temperature profiles at Z = -0.09 m for the air-fired CHT, EGR CHT and EGR CHT + RHT cases (left) and radial temperature profiles at Z = -0.04 m for the adiabatic EGR and the CHT EGR cases (right)

baseline case, it can be observed that the CO_2 concentration in the exhaust gas increases from 1.65% to 5.62%, with all the related beneficial effects for the carbon dioxide separation process. Also, the peak flame temperature is reduced by up to about 70 K. This has an impact on the NO_x emissions, which are significantly reduced with respect to the baseline case. The carbon monoxide levels under the considered EGR ratio are only slightly higher than those calculated for the air-fired-case. This indicates that the combustion efficiency is not significantly affected by CO_2 dilution in this case. As a result of the higher CO_2 heat capacity, the turbine inlet temperature is slightly reduced with respect to the values calculated for the air-fired case.

5. Conclusions

CFD modelling of the combustion process within industrial gas turbine combustors is of paramount importance to assess the effects of EGR on these devices. A 4% carbon dioxide dilution in the oxidizer stream of an industrial micro gas turbine combustor has been considered in the present study to investigate its operation under EGR conditions. An advanced flamelet model with a detailed chemical mechanism for natural gas combustion has been employed to model the combustion process and to account for the effects of CO_2 dilution on the combustion chemistry.

It has been observed that the conjugate heat transfer has a substantial impact on the overall heat transfer within the combustor in both the baseline and the EGR cases, and therefore it must be accounted for in the modelling of DLE combustors. The radiative heat transfer has been found to have a much smaller impact with respect to the conjugate heat transfer. Further, despite the higher concentration of CO_2 and H_2O, the radiative heat transfer is not significantly enhanced in the EGR case with respect to the air-fired condition. This can be

due to the radiative characteristics of the considered configuration as well as to shortcomings in the radiation model under EGR conditions.

Also, it has been found that the resulting higher CO_2 concentration in the combustion environment with EGR has a substantial impact on the combustion process, due to both thermal and chemical effects. As a consequence CO_2 dilution lowers the temperature levels in the combustor by up to about 70 K, thus allowing a significant reduction of the thermal NO_x production. Neither a substantial increase in CO production nor a reduction of the combustion efficiency have been observed.

Further, the increased CO_2 concentration has been found to cause a reduction in the flame speed that, together with the effects of carbon dioxide dilution on the velocity field, led to a change of the axial location of the flame stabilization point.

The present numerical analysis has shown that EGR can be a viable technique to enhance the efficiency of the post-combustion CO_2 capture process by increasing the carbon dioxide content in the exhaust gas of DLE combustors. Also, the operation with EGR results in lower temperature levels, and therefore in reduced NO_x emissions, while maintaining reasonably low CO emissions under the considered conditions. Carbon dioxide dilution has also been observed to have an impact on both the flame speed and the flame stabilization mechanism. In particular, the observed reduction in the flame speed means that the device working point is closer to the lean flammability limit. Thus, even if in the present combustor and under the conditions considered in this study the flame has been observed to be stable, a particular attention has to be paid to flame sustainability and stability when operating DLE combustors with EGR.

Acknowledgement

The authors acknowledge funding from EPSRC grant reference EP/J020788/1: "Gas-FACTS: Gas - Future Advanced Capture Technology Options"

Ali, U., Best, T., Finney, K. N., Palma, C. F., Hughes, K. J., Ingham, D. B., and Pourkashanian, M. (2014). Process simulation and thermodynamic analysis of a micro turbine with post-combustion CO2 capture and exhaust gas recirculation. *Energy Procedia*, 63(44):986–996.

Andersson, K. and Johnsson, F. (2007). Flame and radiation characteristics of gas-fired O2 - CO2 combustion. *Fuel*, 86:656–668.

ANSYS, Inc. (2014). *ANSYS Fluent theory guide - Release 15.0*.

Baltasar, J., Carvalho, M. G., Coelho, P., and Costa, M. (1997). Flue gas recirculation in a gas-fired laboratory furnace: measurements and modelling. *Fuel*, 76:919–929.

Bilger, R. W., Pope, S. B., Bray, K. N. C., and Driscoll, J. F. (2005). Paradigms in turbulent combustion research. *Proceedings of the Combustion Institute*, 30:21–42.

Borghi, R. (1985). On the structure and morphology of turbulent premixed flames. In *Recent advances in Aerospace Sciences*, pages 117–138. Plenum Press, New York.

Boudier, G., Gicquel, L., and Poinsot, T. (2008). Effects of mesh resolution on large eddy simulation of reacting flows in complex geometry combustors. *Combustion and Flame*, 155:196–214.

Bowman, C. T. (1991). Chemistry of gaseous pollutant formation and destruction. In Bartok, W. and Sarofim, A., editors, *Fossil fuel combustion*. J. Wiley and Sons.

Chterev, I., Foley, C. W., Foti, D., Kostka, S., Caswell, a. W., Jiang, N., Lynch, a., Noble, D. R., Menon, S., Seitzman, J. M., and Lieuwen, T. (2014). Flame and flow topologies in an annular swirling flow. *Combustion Science and Technology*, 186(8):1041–1074.

Clements, A. G., Black, S., Szuhánszki, J., Stęchły, K., Pranzitelli, A., Nimmo, W., and Pourkashanian, M. (2015). LES and RANS of air and oxy-coal combustion in a pilot-scale facility: Predictions of radiative heat transfer. *Fuel*, 151:146–155.

De Soete, G. G. (1975). Overall reaction rates of NO and N2 formation from fuel nitrogen. *Symposium (International) on Combustion*, 15(1):1093–1102.

Dodds, W. J. and Bahr, D. W. (1990). *Design of modern gas turbine combustors*. Academic Press Ltd.

ElKady, A. M., Evulet, A., Brand, A., Ursin, T. P., and Lynghjem, A. (2009). Application of exhaust gas recirculation in a DLN F-Class combustion system for postcombustion carbon capture. *Journal of Engineering for Gas Turbines and Power*, 131:51–55.

Gas Research Intitute (2000). *GRI Mechanism version 3.0*. http://www.me.berkeley.edu/gri-mech/.

Goodwin, D. G., Moffat, H. K., and Speth, R. L. (2015). Cantera: An object-oriented software toolkit for chemical kinetics, thermodynamics, and transport processes. Version 2.2.0.

Habib, M. A., Nemitallah, M. A., and Ben-Mansour, R. (2013). Recent development in oxy-combustion technology and its application to gas turbine combustors and ITM reactors. *Energy and Fuels*, 27:2–19.

Hanson, R. K. and Salimian, S. (1984). Survey of rate constants in h/n/o systems. In Gardiner, W., editor, *Combustion chemistry*. Springer.

Hinton, N. and Stone, R. (2014). Laminar burning velocity measurements of methane and carbon dioxide mixtures (biogas) over wide ranging temperatures and pressures. *Fuel*, 116:743–750.

IEA/UNIDO (2013). *Tehcnology roadmap: Carbon Capture and Storage in industrial applications*. IEA Publications.

Jakirlic, S., Hanjalic, K., and Tropea, C. (2002). Modeling rotating and swirling turbulent flows: a perpetual challange. *AIAA Journal*, 40:1984–1996.

Jansohn, P., Griffin, T., Mantzaras, I., Marechal, F., and Clemens, F. (2011). Technologies for gas turbine power generation with CO2 mitigation. *Energy Procedia*, 4:1901–1908.

Kadoya, K., Matsunaga, N., and Nagashima, A. (1985). Viscosity and thermal conductivity of dry air in the gaseous phase. *Journal of Physical and Chemical Reference Data*, 14:947–970.

Li, H., Haugen, G., Ditaranto, M., Berstad, D., and Jordal, K. (2011). Impacts of exhaust gas recirculation (EGR) on the natural gas combined cycle integrated with chemical absorption CO2 capture technology. *Energy Procedia*, 4:1411–1418.

Malte, P. C. and Pratt, D. T. (1975). Measurement of atomic oxygen and nitrogen oxides in jet-stirred combustion. *Symposium (International) on Combustion*, 15(1):1061–1070.

Røkke, P. E. and Hustad, J. E. (2005). Exhaust Gas Recirculation in gas turbines for reduction of CO2 emissions; combustion testing with focus on stability and emissions. *International Journal of Termodynamics*, 8(4):167–173.

Sabia, P., Lubrano Lavadera, M., Giudicianni, P., Sorrentino, G., Ragucci, R., and de Joannon, M. (2015). CO2 and H2O effect on propane auto-ignition delay times under mild combustion operative conditions. *Combustion and Flame*, 162(3):533–543.

Shih, T., Liou, W. W., Shabbir, A., Yang, Z., and Zhu, J. (1995). A new $k-\epsilon$ eddy viscosity model for high reynolds number turbulent flows. *Computers and Fluids*, 24:227–238.

Smith, T. F., Shen, Z. F., and Friedman, J. N. (1982). Evaluation of coefficients for the weighted sum of gray gases model. *Journal of Heat Transfer*, 104:602–608.

Tanaka, Y., Nose, M., Nakao, M., Saitoh, K., Ito, E., and Tsukagoshi, K. (2013). Development of low NOx combustion system with EGR for 1700 C-Class gas turbine. *Mitsubishi Heavy Industries Technical Reviews*, 50(1):1–6.

van Oijen, J. A. (2002). *Flamelet generated manifolds: development and application to premixed laminar flames*. PhD thesis, Eindhoven University of Technology.

van Oijen, J. A. and de Goey, L. P. H. (2000). Modelling of premixed laminar flames using flamelet-generated manifolds. *Combustion Science and Technology*, 161:113–137.

Xie, Y., Wang, J., Zhang, M., Gong, J., Jin, W., and Huang, Z. (2013). Experimental and numerical study on laminar flame characteristics of methane oxy-fuel mixtures highly diluted with CO2. *Energy and Fuels*, 27(10):6231–6237.